Thermal conductivity of Fe graphitized wood derived carbon

J. Ramirez-Rico[1,2*], A. Gutierrez-Pardo[1,2], J. Martinez-Fernandez[1,2], V. V. Popov[3], T. S. Orlova[3]

[1]Departamento Física de la Materia Condensada - ICMS (Universidad de Sevilla-CSIC), Avda. Reina Mercedes S/N, 41012 Seville, Spain.

[2]Instituto de Ciencia de Materiales de Sevilla (CSIC-Univ. Sevilla), Avda. Américo Vespucio 49, 41092 Seville, Spain.

[3]Ioffe Physical-Technical Institute, Russian Academy of Sciences, Politekhnicheskaya ul. 26, 194021 St. Petersburg, Russia

Abstract

Graphitic porous carbon materials from pyrolysis of wood precursors were obtained by means of a nanosized Fe catalyst, and their microstructure and electrical and thermal transport properties investigated. Thermal and electrical conductivity of graphitized carbon materials increase with the pyrolysis temperature, indicating a relationship between the degree of graphitization and thus in crystallite size with transport properties in the resulting carbon scaffolds. Evaluation of the experimental results indicate that thermal conductivity is mainly through phonons and decreases with the temperature in Fe-catalyzed carbons suggesting that due to defect scattering the mean free path of phonons in the material is small and defect scattering dominates over phonon-phonon interactions in the range from room temperature to 800ºC.

Keywords: Carbon materials, graphite, pyrolysis, thermal conductivity, biomorphic materials.

1 Introduction

The interest in materials for thermal management has recently grown by practical issues in engineering. High thermal conductivity has become an essential need for ongoing progress in the electronic industry due to increased levels of dissipated power in many devices [1, 2]. In addition, materials with low densities are desirable in many applications (i.e. cellular, laptops, avionic) while maintaining low production costs is

* corresponding author: [jrr@us.es, Tel. +34 954 550963]

key. As conventional materials used in electronic packaging do not meet all these conditions, new materials have been and are continuing to be developed to accomplish these requirements [2-5].

Carbon materials cover an impressive range of thermal conductivities at room temperature of over five orders of magnitude [1]. While amorphous carbons have conductivities as low as ~0.005 W $(m \cdot K)^{-1}$ and can be used as materials for thermal insulation in a wide range of temperatures [6], diamond is the best bulk heat conductor [7]. Graphite has been the material most rigorously studied to understand its thermal properties and provides references to study the thermal behavior of nanostructured materials [8]. A large number of composites containing a carbon phase with enhanced thermal conductivities have been recently investigated as promising materials in this sense [9-12].

The development of novel scaffold structures by mimicking the cellular anatomy of biostructures has become a topic in materials science research [13-16]. The wide variety of natural precursors available offers a diversity of microstructures, from macroscale to nanoscale [17, 18], and consequently allows for a large range of properties that solve scientific and technical problems [19]. Biomorphic graphitic monoliths have received recent interest due to the desirable thermal [5, 20, 21] and structural [22, 23] properties of porous graphite. Catalytic graphitization is extensively employed since the 80s to produce graphitic structures with the aid of transition-metals [24-26], and the catalytic mechanisms have been also investigated intensely [27, 28]. Carbon obtained by pyrolysis of cellulosic precursors is hard or isotropic, and exhibits a degree of structural disorder that prevents its subsequent graphitization [29], however the transition metal induces graphitization *in situ* within solid carbon materials during the pyrolysis process at moderate temperatures [24, 30, 31]. Subsequently the catalyst particles are removed to obtain a monolithic, graphitic carbon material that combines the properties of pyrolysis-derived carbons, such as low density and aligned, hierarchical porosity [32, 33] with the properties of graphite, such as high degree of ordering, low thermal expansion and good thermal and electrical conductivities [24] making them ideal candidates for many thermal management applications. Thermal properties of wood-derived materials have been reported for ceramics [34], composites [35] and carbons [36].

In contrast to carbon powders, the obtained porous graphitic monoliths retain mecanical strength and exhibit high permeability and interconnectivity, while the continuous solid phase results in good transport properties without the need to use additives or binders [37, 38]. Besides the improvement in capacitances of Fe-catalyzed carbons respect to non-catalyzed carbons – up to two orders of magnitude – for its use as electrodes in electrochemical energy storage [38], these graphitic monolithic structures appear to be a promising material for high temperature thermal management. Other possible applications of these materials are hydrogen storage [39], catalysis [40] or separation processes [41].

The issue of catalytic graphitization, although widely studied due to its importance in the synthesis of carbon nanostructures, is itself still a subject of debate. Graphitization by transition metals, notably Fe, Co or Ni, has been studied in the greatest detail [37, 42-46], and most authors quote a mechanism involving the formation of near eutectic liquid droplets of M_xC_y (where M stands for the metal atom) that continuously dissolve and reprecipitate the surrounding amorphos matrix, yielding a variety of graphitic structures depending on the droplet size [27, 47], that can vary from onion-like nanostructures to bulk, micron sized graphite crystals. Some authors detect the presence of iron carbides after reaction completion and cooling down to room temperature [31], while others do not, rising question as to wether the final structure is formed at high temperature or upon cooling. Open questions in this model are an explanation for the formation temperature of these droplets, which is much lower than that predicted by the respective phase diagrams, as well as their supersaturation [28]. In-situ XPS studies of carbon nanotube growth on ZrO_2 nanoparticles have however shown that graphitization from oxides can proceed without a prior carbothermal reduction to free metal, raising questions about the validity of the aforementioned theories [48].

The aim of this paper is evaluate the effect of pyrolysis temperature on the degree of graphitization as well as on the thermal properties of Fe-catalyzed wood derived carbons, and determine the concurrent phenomena that predict the thermal transport in these carbon scaffolds. The microstructure, density, long- and short-range ordering and both electrical and thermal conductivity ranging from room temperature to 800 ºC of the resulting graphitic monolithic carbons were studied.

2 Experimental

2.1 Materials

Wood-derived carbons were produced from beech (*Fagus silvatica*) wood cut into blocks with dimensions ca. (15 x 15 x 75) mm^3 and stored in a stove at 90ºC until used. Prior to pyrolysis, these blocks were impregnated in a 3M $FeCl_3$ solution in isopropanol in vacuum for 2 hours to ensure complete filling of the pores. Subsequently, the wood samples were heated until completely dry as evaluated by periodic weight measurements. The pyrolysis process took place in a tube furnace with a controlled and constant flow of nitrogen. Pyrolysis was carried out with a ramp rate of 1ºC/min to 500ºC; 5ºC/min to maximum temperature, soak time of 30 minutes and 5ºC/min cooling down to room temperature. This temperature program was chosen to ensure that crack free carbon monoliths could be obtained. The pyrolysis temperatures studied were 850, 1000, 1150, 1300, 1500 and 1600 ºC, and were chosen to study the effect of pyrolysis temperature and thus the degree of graphitization on the conductivity. After pyrolysis, the residual iron was removed by stirring in concentrated HNO_3 (69%, Panreac). The resulting biocarbon monoliths were rinsed and stirred in acetone until neutral pH, and then dried.

2.2 Characterization

Scanning electron microscopy (SEM, JEOL 6460-LV) at an operating voltage of 20 keV was applied to observe the microstructure of the carbon scaffolds. Helium pycnometry (Micromeritics Accupyc) and geometrical means were used to measure the density of wood derived carbons pyrolized at different temperatures. X-ray diffraction was carried out in a powder diffractometer (A25 D8 Advance, Bruker) with Cu K_α radiation at an accelerating voltage of 40 kV and a current of 30 mA to determine the crystallinity in the Fe-catalyzed carbons. Raman spectroscopy (LabRam Jobin Yvon) at room temperature was used to determine the degree of structural disorder in the carbon structures using an excitation wavelength of 532 nm, in the spectral region between 1000 and 1800 cm^{-1} which yields the most interesting structural information on carbonaceous materials [49, 50]. Obtained Raman spectra were analyzed using a least-squares fitting code written in-house. Relevant bands typical of carbonaceous materials [50] were fitted to pseudo-Voigt lineshapes and relative widths and intensities calculated. The extent of structural order in the graphitized carbon scaffolds was assessed by calculating the degree of crystallinity β defined as the relative fraction of

the G-band (~1580 cm^{-1}) intensity to the sum of the intensities of bands G and D_1 (~1350 cm^{-1}), according to:

$$\beta = \frac{I_G}{I_G + I_{D_1}} \quad (1)$$

2.3 Thermal conductivity

Thermal diffusivity was measured in the axial direction using the laser flash technique [51] (Linseis LFA1600). Samples of carbon pyrolyzed at different temperatures were cut into squares with a surface of 1 cm^2 and 5 mm thick and spray coated with colloidal graphite to prevent the direct laser radiation reaching the InSb infrared detector. Three measurements were carried out in vacuum at each temperature in the range of 25ºC to 800ºC, with the heat flow direction aligned to the wood precursors' original axis. Reported values correspond to the mean and standard deviation of these three measurements.

In the laser flash technique one side of the sample is irradiated by an infrared laser pulse while the temperature of the other side is measured using an InSb infrared detector. The thermal diffusivity α is calculated following:

$$\alpha = \frac{\omega L^2}{\pi^2 t_{1/2}} \quad (2)$$

Where L is the sample thickness, ω is a constant that accounts for thermal losses [52] and $t_{1/2}$ is the time it takes for the temperature of the opposite side to reach half its maximum value.

Once the diffusivity is known, the thermal conductivity can be calculated using:

$$\kappa(T) = \alpha(T) C_p(T) \rho \quad (3)$$

In the equation (3) ρ is the sample density and $C_p \approx C_v$ is the specific heat capacity of the material at constant pressure. In our measurements, ρ was taken as the solid density while the heat capacity was taken from the literature [53].

2.4 Electrical conductivity

Room temperature electrical conductivity was measured using standard four-probe techniques. The sample size was (3 × 3 × 20) mm^3; long sides were oriented along the

primary tree growth direction (along channel pores). In measuring the resistivity the electric current flowed along the long sample side, i.e., in parallel to channel pores.

3 Results and discussion

3.1 Structural characterization

SEM images for Fe-catalyzed carbons pyrolyzed at 1300ºC before catalyst removal are shown in Figure 1, both using secondary electrons to show the microstructure of the carbon scaffold as well as backscattered electrons to reveal the size and morphology of the catalyst nanoparticles. The microstructure of the carbon monolith replicates that of the original wood, consisting of interconnected and aligned channels with a bimodal size distribution. After etching with HNO_3, a soluble salt of iron is formed and catalyst particles are removed from the material. A carbon skeleton which mimics the microstructure of the natural precursor with open and interconnected porosity is thus obtained. All carbon materials show common features in their Raman spectra: the G band (1580 cm^{-1}, E_{2g} symmetry), produced from the high degree of symmetry and order of the graphite lattice, and some D bands caused from the disordered structures. Among them the most interesting band is the D_1 (1350 cm^{-1}, A_{1g} symmetry) which is due to the vibration of graphene layer edges [50] and is the most prominent in amorphous carbon materials.

Figure 2 shows the Raman spectra of some of the samples studied along with the results of the least squares fitting. It can be seen that the relative intensities of the G to D_1 bands increase with increasing pyrolysis temperature while the full width at half maximum of the G band decreases, indicating a higher amount of graphitic carbon in relation to amorphous carbon and therefore an increase of structural order in the material. In un-catalyzed samples it has been shown by X-ray diffraction that the amount of turbostratic carbon increases with increasing temperature [29, 54], which explains the decreasing trend in the G-band FWHM and increase of the G/D_1 ratio. The large decrease in G-band FWHM as well as the large increase in G-band intensity at the onset of graphitization temperature can be then attributed to the presence of three-dimensionally ordered graphite.

To further quantify this effect, we fitted the Raman spectra to the previously described bands using Pseudo-Voigt line shapes, and calculated a degree of crystallinity parameter β as defined previously. This parameter is plotted as a function of pyrolysis temperature

in Figure 3, along with the density of the carbon scaffolds: it can be seen that there is an increase of crystallinity with increasing pyrolysis temperature, and that this increase is steeper in the range of 1100-1400ºC, as it has been shown also for biocarbon graphitized using Ni as a catalyst [37]. This observation is corroborated by our X-ray diffraction results, which are shown in Figure 4. Fe-catalyzed carbons show a peak centered at $2\theta = 26.6°$, corresponding to the (0002) crystal planes of graphite [*pdf 26-1079*]. This peak becomes taller and narrow with increasing pyrolysis temperature, indicating a higher degree of crystallinity. Therefore, the sample pyrolyzed at 1000 °C shows a small and broad peak which indicates the onset of the graphitization, while at 1600 °C the peak is much sharper.

3.2 Thermal conductivity

Measured thermal diffusivities as a function of temperature are plotted in Figure 5 for all pyrolysis temperatures studied. In this figure it can be seen that, at a given temperature, diffusivity increases with increasing pyrolysis temperature, suggesting a relationship between the degree of graphitization and thus crystallinity with transport properties in the resulting carbon scaffold. This hypothesis is further corroborated by our measurements of room temperature electrical conductivity, which are plotted in Figure 6 along room temperature thermal conductivity. As the pyrolysis temperature is increased, both thermal and electrical conductivity increase, suggesting a higher degree of crystalline ordering in materials pyrolyzed at higher temperatures. It has been shown in wood-derived porous carbons that increasing pyrolysis temperature increases the degree of crystalline long-range ordering, both when catalysts are used to promote graphitization [24, 30, 36-38, 55-58] but also when they are not [29, 53, 59-61], by increasing the size of the graphitic regions in the turbostratic carbon layers (increasing crystallite size). In the case of Ni-catalyzed samples, the precipitation of large, micron sized graphite crystals has been observed [24, 37] by transmission electron diffraction, even if they are absent in Fe-catalyzed samples. An increase in crystallite size would enhance transport properties by an increase in the crystalline volume fraction in the material as well as the degree of percolation of the crystalline regions. In the case of thermal transport by phonons, as will be discussed below, the increase on crystallite size would also have the effect of reducing phonon scattering at boundaries and defects.

Thermal conductivity in porous solids can be attributed to three concurrent phenomena: conduction by electrons, conduction by phonons and radiative transfer. The latter has

been shown to be negligible for porous carbon and SiC materials with a microstructure and emissivity resembling that of wood [34, 53] and thus will not be considered further. Then, the total thermal conductivity can be written as:

$$\kappa = \kappa_{electrons} + \kappa_{phonons} \quad (4)$$

The electronic contribution to thermal conductivity depends strongly on carrier concentration and mobility, and is related in a first approximation to electrical conductivity through the Wiedemann-Franz law:

$$\kappa_{electrons}(T) = \sigma T \frac{\pi^2}{3}\left(\frac{k_B}{e}\right)^2 \quad (5)$$

Where σ is the electrical conductity, T is the temperature, k_B is the Boltzmann constant and e is the electron charge.

The phonon contribution to the thermal conductivity has two terms, related to the phonon density and to phonon-phonon interactions (*Umklapp* scattering), following:

$$\kappa_{phonons}^{-1} = \kappa_{capacity}^{-1} + \kappa_{Umklapp}^{-1} \quad (6)$$

The term $\kappa_{capacity}$ is related to phonon density and thus to the heat capacity of the material, according to:

$$\kappa_{capacity} = \frac{1}{3}\rho c_V(T) v_{ph} l \quad (7)$$

Where ρ is the density, $c_V(T)$ is the specific heat capacity, which is temperature dependent and v_{ph} is an average phonon velocity. The remaining parameter, l, is the phonon mean free path, which depends on the concentration of phonon scatterers in the material. The two main phonon scatterers are atomic impurities and grain boundaries/interfaces: a reduction of either impurity concentration or the grain boundary density, by an increase in crystallite size, would enhance thermal conductivity. Since in our case all the studied materials are synthesized with the same conditions, catalyst concentration, etc., it is safe to assume that any change in thermal conductivity associated to a change in pyrolysis temperature should be attributed to an increase in crystallite size only and thus on changes in the phonon mean free path.

The last term is related to *Umklapp* processes, in which phonons are scattered by other phonons. This effect is relevant at high temperatures where phonon density is

approximately constant and thus an increase in temperature results in an increase in the probability of phonon-phonon scattering events. *Umklapp* scattering is usually empirically described by a relationship of the form:

$$\kappa_{Umklapp} \sim \frac{1}{T^x} \quad (8)$$

Where $x = 1 - 2$. An important consequence of the above discussion is that phonon-phonon interactions are essentially independent on crystallite size, and result in a reduction of thermal conductivity with increasing temperature.

Figure 7 shows the thermal conductivities derived from measured diffusivities and densities, and from reference heat capacity [53, 62]. In this case, conductivities increase with increasing temperature and, for a given temperature, also increase with pyrolysis temperature. To evaluate the electronic contribution, we have calculated $\kappa_{electrons}$ using the Wiedeman-Franz law and plotted the result in Figure 7, assuming that the electrical conductivity does not vary with temperature as a first approximation. For ease of viewing, we have only plotted the $\kappa_{electrons}$ contribution calculated for samples pyrolyzed at the highest temperature, 1600ºC; $\kappa_{electrons}$ for the rest of the studied samples would fall below this line. It is clear then that the electronic contribution to conductivity is very small, and thus $\kappa_{phonons}$ should dominate.

In POCO graphite foams, obtained from mesophase pitch and exhibiting a large degree of crystallinity and crystallite size, thermal conductivity is dominated by *Umklapp* scattering in the whole range of temperatures measured here. If that were the case for graphitized wood biocarbon, thermal conductivity should be essentially independent of temperature, which goes against our results, as well as previously reported values for Ni-catalyzed wood derived carbon [36] or resorcinol-formaldehyde derived carbon aerogels [53] which show an increase of conductivity with temperature. This means that mean free path of phonons in these materials is so small that defect scattering dominates over *Umklapp* processes in the range of temperatures studied.

Solid lines in Figure 7 represent the results of fitting the experimental thermal conductivity values to Equation (6). In this case, the influence of phonon-phonon scattering was fitted globally for all pyrolysis temperatures since it should be independent of microstructure and crystallite size in a first approximation. Thus, the only fitting parameter was:

$$A = \frac{1}{3}\rho v_{ph} l \quad (9)$$

Which is temperature independent. The parameter *A* is a multiplicative factor describing the effects of density, phonon mean velocity and free path on κ_{phonon}, which can be calculated from the result of the fit since the rest of the parameters are known or can be obtained from the literature. For the calculation of crystallite size, measured solid densities and a value of $v_{ph} = 725\ m/s$ [53] were used; results are detailed in Table 1, along with the rest of relevant results from this paper. Consistent with previous observations [37, 53, 58, 63, 64], increasing pyrolysis temperature results in an increase in crystallite size to which we attribute the enhancement of transport properties, either thermal or electrical.

It is instructive, to put our results in context, to compare the thermal conductivity of Fe-catalyzed samples with results of similar materials. Figure 8 compares the thermal conductivity reported here with the results of Wiener et al. [53] for polymer derived carbon aerogels as well as results from Johnson et al. for beech derived carbon [36] for both Ni-catalyzed and uncatalyzed samples, measured at 200 ºC. It is clear that, for pyrolysis temperatures under ca. 1000 ºC all results fall under the same range, whereas for higher pyrolysis temperatures a significant increase is observed. The use of a transition metal results in an enhancement in thermal conductivity, higher in the case of Fe graphitized carbon which has been shown to be more efficient at inducing graphitization.

4 Conclusions

Porous graphitic monolithic carbons have been achieved using an iron catalyst during pyrolysis, retaining the microstructure of the wood precursor used. The degree of crystallinity and structural order of Fe-catalyzed samples increases with an increase in the pyrolysis temperature. The increasing of both thermal and electrical conductivity with the pyrolysis temperature confirms an enlargement in crystallite size that enhances the transport properties by an increase in the crystalline volume fraction in the material as well as the degree of percolation of the crystalline regions.

Thermal diffusivity in Fe-catalyzed carbons is dependent on the measured temperature and increases in the range studied, from 25 to 800 ºC. Heat conduction in carbon materials is produced mainly by phonons. Evaluation of the experimental results

attending to the phonon contributions suggests that the mean free path of phonons is so small that defect scattering dominates over *Umklapp* processes in our material. Thermal conductivity of Fe-graphitized carbons is up to 5 times higher than in non-graphitized wood-derived carbons measured at the same conditions.

Acknowledgements.

This work was supported by the Junta de Andalucía under grant PE2012-TEP862 as well as by the Ministry of Economy and Competitivity of the Spanish Government under grant MAT2013-41233-R. Electron microscopy, X-ray diffraction and thermal diffusivity measurements were performed at the CITIUS central services of the University of Seville. Raman scattering measurements were performed at the ICMS (University of Seville-CSIC).

Figure Captions

Figure 1. SEM micrographs of carbon samples pyrolyzed at 1300 ºC after impregnation with Fe, taken using: A) Secondary electrons, B) backscattered electrons to obtain composition contrast highlighting the presence of Fe nanoparticles in the wood pores.

Figure 2. Raman spectra as well as peak fitting results for graphitized carbon samples obtained by pyrolysis at 850, 1000, 1300 and 1600 ºC.

Figure 3. Geometrical density, solid (pycnometer) density and degree of crystallinity β determined by Raman spectroscopy as a function of pyrolysis temperature for Fe-catalyzed beech derived porous carbon.

Figure 4. X-ray diffraction patterns for carbon materials pyrolyzed at different temperatures in presence of the Fe catalyst.

Figure 5. Thermal diffusivity as a function of temperature for Fe-catalyzed carbon materials pyrolyzed at different temperatures.

Figure 6. Room temperature thermal conductivity vs. electrical conductivity for Fe-catalyzed carbon materials pyrolyzed at different temperatures. The red line is included only as a visual aid and does not imply any particular relationship between the two parameters.

Figure 7. Thermal conductivity as a function of temperature for Fe-catalyzed carbon materials pyrolyzed at different temperatures. The dashed line corresponds to the electronic contribution to the thermal conductivity calculated using measured electrical conductivities and the Wiedeman-Franz law. For clarity, only the curve corresponding to a pyrolysis temperature of 1600ºC is shown, the rest fall below this one. Colored lines represent fits to the thermal conductivity assuming that phonon transport dominates, see text for details.

Figure 8. Comparison of room temperature thermal conductivity as a function of pyrolysis temperature. Our data is represented as hollow circles, blue triangles and green circles represent data for beech derived carbon with a Ni-catalyst and without catalyst [36] and red squares represent data obtained from polymer-derived carbon aerogels [53]. Lines are included as a guide to the eye. Temperature is 200ºC for wood derived carbon and 300ºC for carbon aerogels.

Tables

Table 1: Summary of results derived from this work

Pyrolysis Temperature (º C)	Bulk density (g/cm^3)	Solid density (g/cm^3)	RT Thermal conductivity (W/ m·K)	RT Electrical conductivity (S/cm)	Crystallinity ratio β	Crystallite Size (±1 nm)
850	0.59	1.73	0.7	10	0.27	4
1000	0.64	2.03	2.7	29	0.28	11
1150	0.55	2.03	3.9	50	0.31	13
1300	0.53	2.03	3.8	56	0.45	13
1500	0.52	1.70	5.3	66	0.59	18
1600	0.47	1.66	5.4	76	0.63	21

References

[1] Balandin AA. Thermal properties of graphene and nanostructured carbon materials. Nat Mater. 2011;10:569-81.

[2] Zweben C. Advances in composite materials for thermal management in electronic packaging. Jom-Journal of the Minerals Metals & Materials Society. 1998;50:47-51.

[3] Kim P, Shi L, Majumdar A, McEuen P. Thermal transport measurements of individual multiwalled nanotubes. Physical review letters. 2001;87:215502.

[4] Pop E, Mann D, Wang Q, Goodson K, Dai H. Thermal conductance of an individual single-wall carbon nanotube above room temperature. Nano letters. 2006;6:96-100.

[5] Gaies D, Faber K. Thermal properties of pitch-derived graphite foam. Carbon. 2002;40:1137-40.

[6] Wiener M, Reichenauer G, Braxmeier S, Hemberger F, Ebert H-P. Carbon aerogel-based high-temperature thermal insulation. Int J Thermophys. 2009;30:1372-85.

[7] Ho C, Powell R, Liley P. Thermal Conductivity of the Elements: A Comprehensive Review, Vol. 3, Suppl. No 1. J Phys Chem Ref Data. 1974.

[8] Lepri S, Livi R, Politi A. Thermal conduction in classical low-dimensional lattices. Physics Reports. 2003;377:1-80.

[9] Huang Y, Ouyang Q, Guo Q, Guo X, Zhang G, Zhang D. Graphite film/aluminum laminate composites with ultrahigh thermal conductivity for thermal management applications. Materials & Design. 2016;90:508-15.

[10] Yu G-C, Wu L-Z, Feng L-J. Enhancing the thermal conductivity of carbon fiber reinforced polymer composite laminates by coating highly oriented graphite films. Materials & Design. 2015;88:1063-70.

[11] Chen J, Xiao P, Xiong X. The mechanical properties and thermal conductivity of carbon/carbon composites with the fiber/matrix interface modified by silicon carbide nanofibers. Materials & Design. 2015;84:285-90.

[12] Jana P, Fierro V, Pizzi A, Celzard A. Thermal conductivity improvement of composite carbon foams based on tannin-based disordered carbon matrix and graphite fillers. Materials & Design. 2015;83:635-43.

[13] Greil P, Lifka T, Kaindl A. Biomorphic cellular silicon carbide ceramics from wood: I. Processing and microstructure. J Eur Ceram Soc. 1998;18:1961-73.

[14] Greil P. Biomorphous ceramics from lignocellulosics. J Eur Ceram Soc. 2001;21:105-18.

[15] Schnepp Z, Yang W, Antonietti M, Giordano C. Biotemplating of Metal Carbide Microstructures: The Magnetic Leaf. Angew Chem Int Edit. 2010;49:6564-6.

[16] Wu S, Liu X, Yeung KW, Liu C, Yang X. Biomimetic porous scaffolds for bone tissue engineering. Materials Science and Engineering: R: Reports. 2014;80:1-36.

[17] Kaul V, Faber K, Sepulveda R, de Arellano López A, Martinez-Fernandez J. Precursor selection and its role in the mechanical properties of porous SiC derived from wood. Materials Science and Engineering: A. 2006;428:225-32.

[18] Chen P-Y, McKittrick J, Meyers MA. Biological materials: functional adaptations and bioinspired designs. Progress in Materials Science. 2012;57:1492-704.

[19] Zhang Q, Yang X, Li P, Huang G, Feng S, Shen C, et al. Bioinspired engineering of honeycomb structure–Using nature to inspire human innovation. Progress in Materials Science. 2015;74:332-400.

[20] Klett J, Hardy R, Romine E, Walls C, Burchell T. High-thermal-conductivity, mesophase-pitch-derived carbon foams: effect of precursor on structure and properties. Carbon. 2000;38:953-73.

[21] Wang S, Morelos-Gómez A, Lei Z, Terrones M, Takeuchi K, Sugimoto W, et al. Correlation in structure and properties of highly-porous graphene monoliths studied with a thermal treatment method. Carbon. 2016;96:174-83.

[22] Zhou Z, Bouwman WG, Schut H, Desert S, Jestin J, Hartmann S, et al. From nanopores to macropores: Fractal morphology of graphite. Carbon. 2016;96:541-7.

[23] Canseco V, Anguy Y, Roa JJ, Palomo E. Structural and mechanical characterization of graphite foam/phase change material composites. Carbon. 2014;74:266-81.

[24] Johnson MT, Faber KT. Catalytic graphitization of three-dimensional wood-derived porous scaffolds. J Mater Res. 2011;26:18-25.

[25] Liu Y, Liu Q, Gu J, Kang D, Zhou F, Zhang W, et al. Highly porous graphitic materials prepared by catalytic graphitization. Carbon. 2013;64:132-40.

[26] Zhai D, Du H, Li B, Zhu Y, Kang F. Porous graphitic carbons prepared by combining chemical activation with catalytic graphitization. Carbon. 2011;49:725-9.

[27] Glatzel S, Schnepp Z, Giordano C. From Paper to Structured Carbon Electrodes by Inkjet Printing. Angew Chem Int Edit. 2013;52:2355-8.

[28] Feng XF, Chee SW, Sharma R, Liu K, Xie X, Li QQ, et al. In Situ TEM observation of the gasification and growth of carbon nanotubes using iron catalysts. Nano Res. 2011;4:767-79.

[29] Pappacena KE, Gentry SP, Wilkes TE, Johnson MT, Xie S, Davis A, et al. Effect of pyrolyzation temperature on wood-derived carbon and silicon carbide. J Eur Ceram Soc. 2009;29:3069-77.

[30] Oya A, Marsh H. Phenomena of Catalytic Graphitization. J Mater Sci. 1982;17:309-22.

[31] Thompson E, Danks A, Bourgeois L, Schnepp Z. Iron-catalyzed graphitization of biomass. Green Chemistry. 2015;17:551-6.

[32] Byrne CE, Nagle DC. Cellulose derived composites - A new method for materials processing. Mater Res Innov. 1997;1:137-44.

[33] Byrne CE, Nagle DC. Carbonization of wood for advanced materials applications. Carbon. 1997;35:259-66.

[34] Pappacena KE, Faber KT, Wang H, Porter WD. Thermal conductivity of porous silicon carbide derived from wood precursors. J Am Ceram Soc. 2007;90:2855-62.

[35] Pappacena KE, Johnson MT, Wang H, Porter WD, Faber KT. Thermal properties of wood-derived copper-silicon carbide composites fabricated via electrodeposition. Compos Sci Technol. 2010;70:478-84.

[36] Johnson MT, Childers AS, Ramirez-Rico J, Wang H, Faber KT. Thermal conductivity of wood-derived graphite and copper-graphite composites produced via electrodeposition. Compos Part a-Appl S. 2013;53:182-9.

[37] Gutierrez-Pardo A, Ramirez-Rico J, de Arellano-Lopez AR, Martinez-Fernandez J. Characterization of porous graphitic monoliths from pyrolyzed wood. J Mater Sci. 2014;49:7688-96.

[38] Gutierrez-Pardo A, Ramirez-Rico J, Cabezas-Rodriguez R, Martinez-Fernandez J. Effect of catalytic graphitization on the electrochemical behavior of wood derived carbons for use in supercapacitors. J Power Sources. 2015;278:18-26.

[39] Sevilla M, Fuertes AB, Mokaya R. Preparation and hydrogen storage capacity of highly porous activated carbon materials derived from polythiophene. Int J Hydrogen Energ. 2011;36:15658-63.

[40] Church TL, Fallani S, Liu J, Zhao M, Harris AT. Novel biomorphic Ni/SiC catalysts that enhance cellulose conversion to hydrogen. Catal Today. 2012;190:98-106.

[41] Eltmimi AH, Barron L, Rafferty A, Hanrahan JP, Fedyanina O, Nesterenko E, et al. Preparation, characterisation and modification of carbon-based monolithic rods for chromatographic applications. J Sep Sci. 2010;33:1231-43.

[42] Sevilla M, Fuertes AB. Catalytic graphitization of templated mesoporous carbons. Carbon. 2006;44:468-74.

[43] Sevilla M, Sanchis C, Valdes-Solis T, Morallon E, Fuertes AB. Synthesis of graphitic carbon nanostructures from sawdust and their application as electrocatalyst supports. J Phys Chem C. 2007;111:9749-56.

[44] Gorria P, Fernandez-Garcia MP, Sevilla M, Blanco JA, Fuertes AB. Nickel nanoparticles deposited into an activated porous carbon: synthesis, microstructure and magnetic properties. Phys Status Solidi-R. 2009;3:4-6.

[45] Sevilla M, Fuertes AB. Graphitic carbon nanostructures from cellulose. Chem Phys Lett. 2010;490:63-8.

[46] Sevilla M, Fuertes AB. Fabrication of porous carbon monoliths with a graphitic framework. Carbon. 2013;56:155-66.

[47] Krivoruchko OP, Zaikovskii VI. A new phenomenon involving the formation of liquid mobile metal-carbon particles in the low-temperature catalytic graphitisation of amorphous carbon by metallic Fe, Co and Ni. Mendeleev Commun. 1998:97-100.

[48] Steiner SA, Baumann TF, Bayer BC, Blume R, Worsley MA, MoberlyChan WJ, et al. Nanoscale Zirconia as a Nonmetallic Catalyst for Graphitization of Carbon and Growth of Single- and Multiwall Carbon Nanotubes. J Am Chem Soc. 2009;131:12144-54.

[49] Cai YB, Hu Y, Song L, Xuan SY, Zhang Y, Chen ZY, et al. Catalyzing carbonization function of ferric chloride based on acrylonitrile-butadiene-styrene copolymer/organophilic montmorillonite nanocomposites. Polym Degrad Stabil. 2007;92:490-6.

[50] Sadezky A, Muckenhuber H, Grothe H, Niessner R, Poschl U. Raman micro spectroscopy of soot and related carbonaceous materials: Spectral analysis and structural information. Carbon. 2005;43:1731-42.

[51] Parker WJ, Jenkins RJ, Abbott GL, Butler CP. Flash Method of Determining Thermal Diffusivity, Heat Capacity, and Thermal Conductivity. J Appl Phys. 1961;32:1679-&.

[52] Clark LM, Taylor RE. Radiation Loss in Flash Method for Thermal-Diffusivity. J Appl Phys. 1975;46:714-9.

[53] Wiener M, Reichenauer G, Hemberger F, Ebert HP. Thermal conductivity of carbon aerogels as a function of pyrolysis temperature. Int J Thermophys. 2006;27:1826-43.

[54] Kercher AK, Nagle DC. Microstructural evolution during charcoal carbonization by X-ray diffraction analysis. Carbon. 2003;41:15-27.

[55] Oya A, Otani S. Catalytic Graphitization of Carbons by Various Metals. Carbon. 1979;17:131-7.

[56] Oya A, Yoshida S, Alcanizmonge J, Linaressolano A. Formation of Mesopores in Phenolic Resin-Derived Carbon-Fiber by Catalytic Activation Using Cobalt. Carbon. 1995;33:1085-90.

[57] Popov VV, Orlova TS, Gutierrez-Pardo A, Ramirez-Rico J. Specific features of the electrical properties in partially graphitized porous biocarbons of beech wood. Phys Solid State+. 2015;57:1746-51.

[58] Orlova TS, Kardashev BK, Smirnov BI, Gutierrez-Pardo A, Ramirez-Rico J, Martinez-Fernandez J. Microstructure, elastic and inelastic properties of partially graphitized biomorphic carbons. Phys Solid State+. 2015;57:586-91.

[59] Parfen'eva LS, Orlova TS, Smirnov BI, Smirnov IA, Misiorek H, Jezowski A, et al. Thermal conductivity at the amorphous-nanocrystalline phase transition in beech wood biocarbon. Phys Solid State+. 2014;56:1071-80.

[60] Parfen'eva L, Orlova T, Kartenko N, Sharenkova N, Smirnov B, Smirnov I, et al. Thermal conductivity of high-porosity biocarbon preforms of beech wood. Phys Solid State+. 2010;52:1115-22.

[61] Kartenko N, Orlova T, Parfen'eva L, Smirnov B, Smirnov I. Thermal conductivity of the amorphous and nanocrystalline phases of the beech wood biocarbon nanocomposite. Phys Solid State+. 2014;56:2348-52.

[62] Taylor RE, Groot H. Thermophysical Properties of POCO Graphite. DTIC Document; 1978.

[63] Kardashev BK, Orlova TS, Smirnov BI, Wilkes TE, Faber KT. Young's modulus and internal friction in porous biocarbon white pine wood precursors. Phys Solid State+. 2009;51:2463-8.

[64] Shpeizman VV, Orlova TS, Kardashev BK, Smirnov BI, Gutierrez-Pardo A, Ramirez-Rico J. Effect of carbonization temperature on the microplasticity of wood-derived biocarbon. Phys Solid State+. 2014;56:538-45.

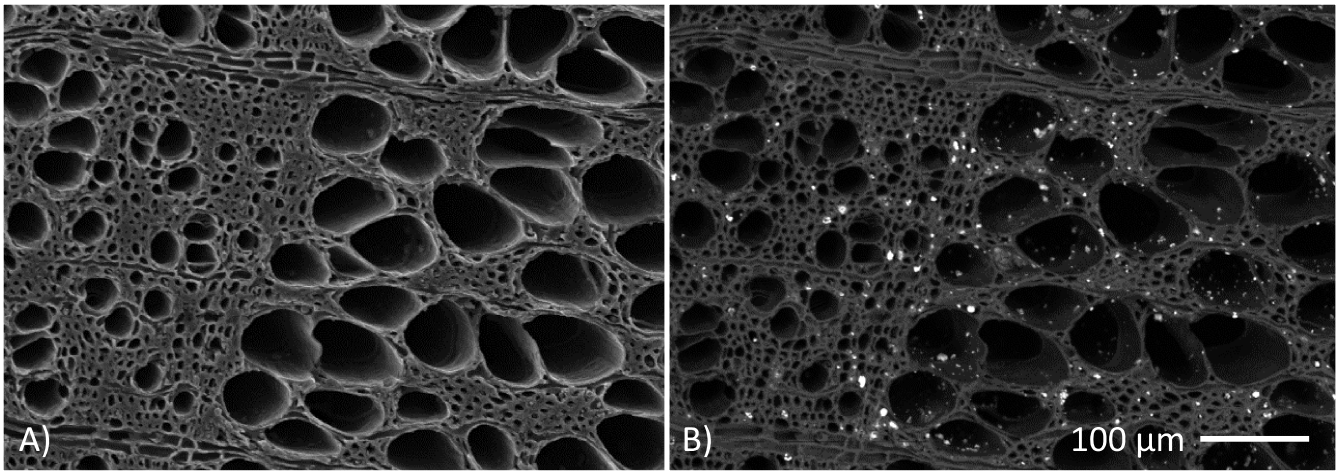

Figure 1

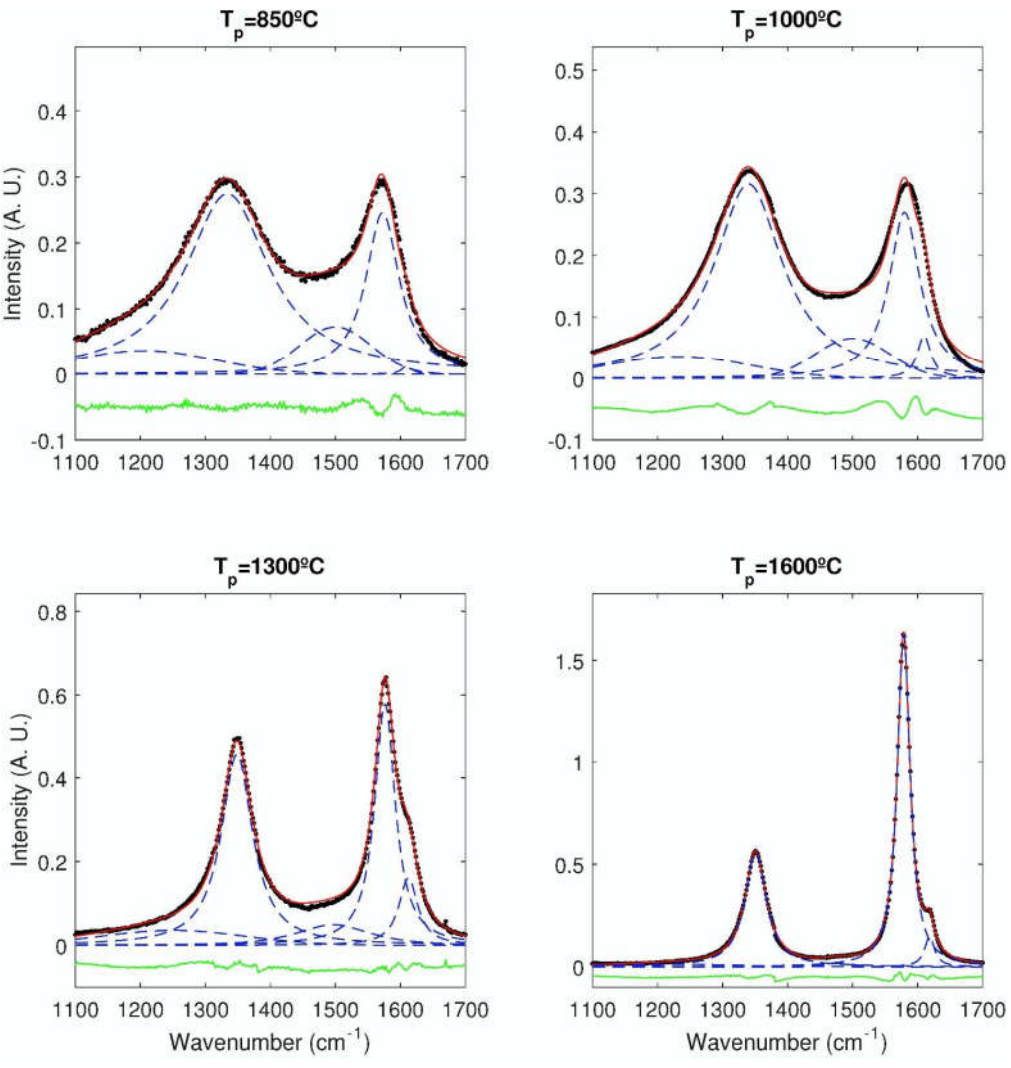

Figure 2

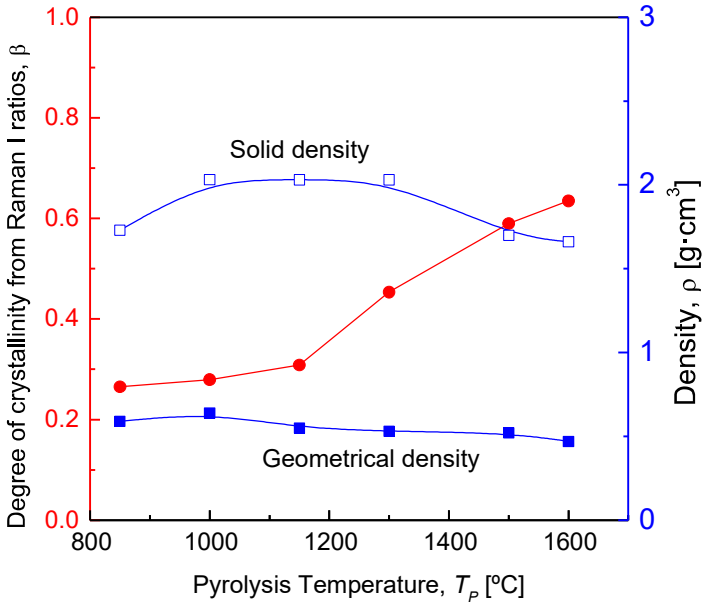

Figure 3

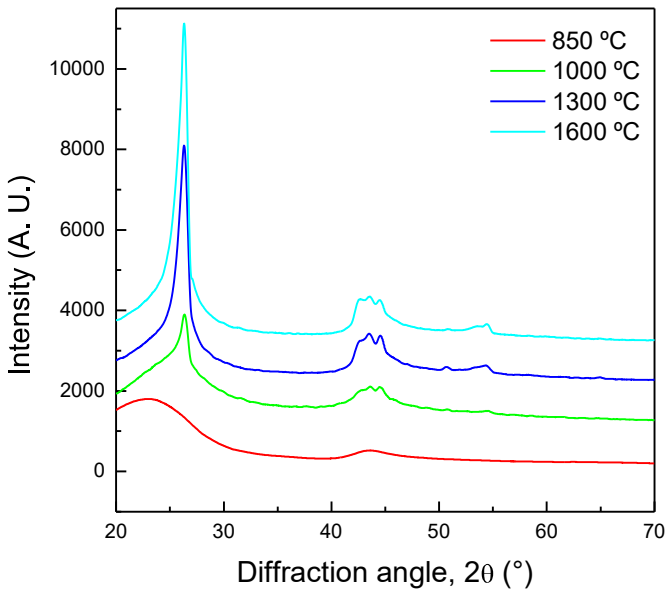

Figure 4

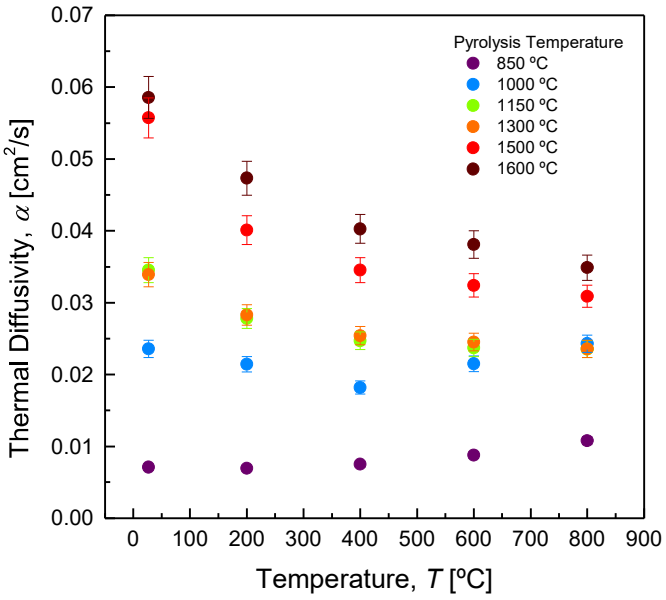

Figure 5

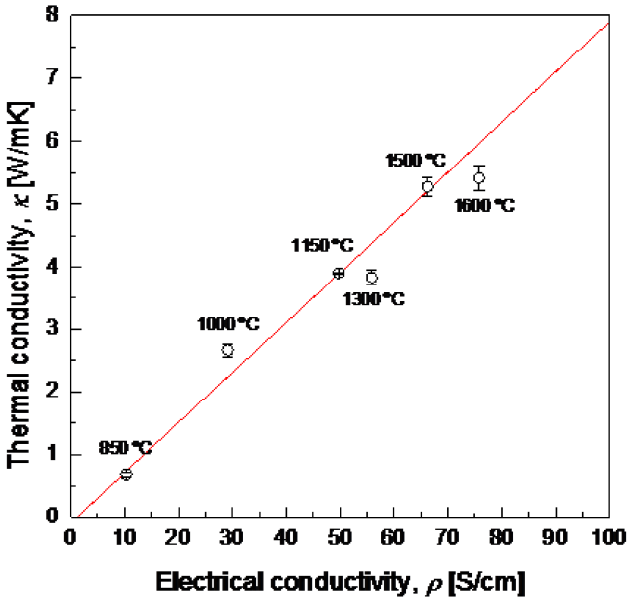

Figure 6

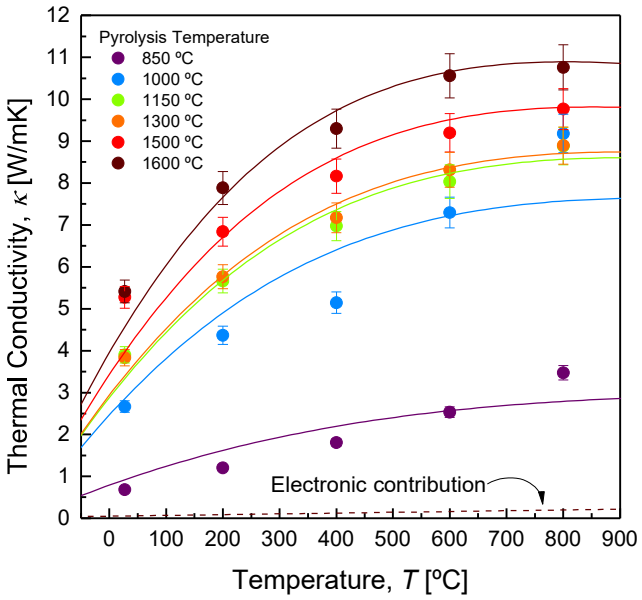

Figure 7

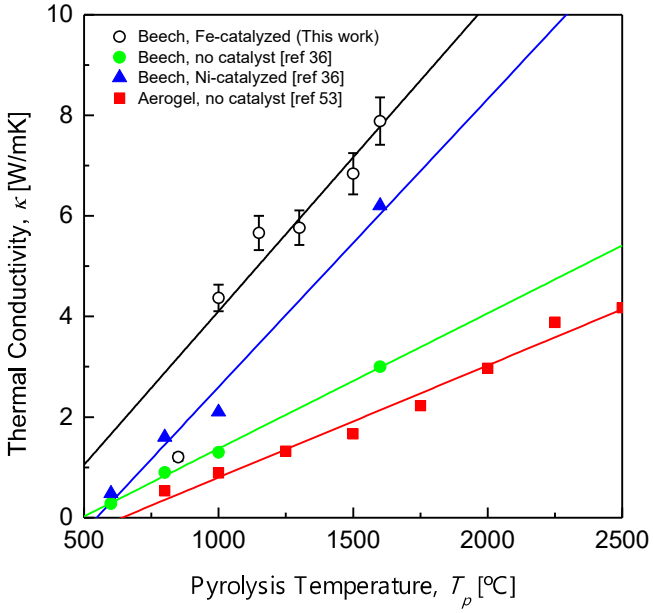

Figure 8